Bicycle Wheel Spoke Patterns and Spoke Fatigue [1]

Henri P. Gavin, Associate Member ASCE[2]

Keywords: circular arch, field tests, prestressing, probability theory, safety, spokes, tests, vehicles

ABSTRACT

The radial, lateral, and tangential stiffness of spoked bicycle wheels depends upon the rim's bending inertia, torsional inertia, the spoke sizes, and the spoke geometry. The spokes of three rear bicycle wheels of different spoke patterns were instrumented with strain gauges in order to investigate the effect of the spoke pattern on the spoke strain and fatigue resistance properties of the wheels. Spoke strains due to radial loads were measured in the laboratory. Time-records of the strain of a right pulling spoke were collected from each of the wheels under actual riding conditions. Analytical, numerical, laboratory, and field studies show that spoke strains due to radial loads and in service conditions are insensitive to the spoke pattern. Small variations in the spoke strains between the wheels in the road tests can be attributed to variations in the loads, but do not significantly affect the fatigue life of the wheels.

INTRODUCTION

Spoked bicycle wheels are efficient, highly evolved, structural systems. A useful analogy for a bicycle wheel supporting vertical loads is that of a circular beam on a prestressed elastic foundation, fixed at the center and loaded radially at the circumference. To apply this analogy, the system of interlacing spokes can be modeled as a disk of uniform stiffness per length of circumference. Spokes of varying lengths may be laced into wheels of fixed dimensions, by modifying the interlacing geometry of the spokes. The connection of the spoke to the hub is accomplished via a cold-worked right angle elbow in the spoke and a flanging of the spoke material. Most spoke failures occur at this fatigue critical detail. Upon the failure of one spoke, ensuing unbalanced lateral forces on the rim result in large lateral deformations of the rim, which may precipitate lateral buckling of the wheel, or failure of other spokes. A loose spoke can interfere with the smooth operation of the chain, which may result in a lost race, a collision, or an injury.

Variations in radial stiffness due to the spoke pattern, calculated using the theory of circular beams on elastic foundations, agree with those using a three-dimensional elastic frame analysis. While the spoke lacing pattern influences the over-all stiffness of the wheel, the strains in spokes at the loading point on the rim are not as sensitive to the spoke pattern. Static tests on three identical rear wheels, with different spoke lengths, also show that spoke strains are not strongly affected by the spoke pattern. Strain time-histories collected during road tests also show only small differences between the wheel types. The fatigue life of the spokes of a rear wheel supporting radial loads is therefore not significantly influenced by the spoke pattern. Spoke strain time histories, collected under actual road conditions, are used to evaluate the fatigue reliability of the three wheels. This study shows that spoked bicycle wheels have high reliability against fatigue failure.

PROPERTIES OF WHEELS USED IN EXPERIMENTS

Asymmetry about a plane through the rim of most rear bicycle wheels provides clearance for the free-wheel on the right side of the wheel. The right flange of the hub is closer to the plane through the

[1] *ASCE Journal of Engineering Mechanics*, vol 122, no. 8, (August 1996) pp. 736–742.

[2] Assistant Professor, Department of Civil Engineering, Duke University, Durham, NC 27708–0287 Tel: (919) 660–5201

rim than is the left flange. The pre-tensioning stresses of the right spokes can be up to three times the pre-tensioning stresses of the left spokes to balance the lateral forces on the rim.

The pattern in which spokes are laced into a wheel affects performance measures such as stiffness, mass, and energy absorption. Wheels with a greater number of spoke crossings have longer spokes which are more tangential to the hub. Figure 1 shows the spokes connected to one hub flange. Wheels are distinguished by the number of times a spoke crosses other spokes: 2X, 3X, and 4X. Radially spoked wheels are designated: 0X. In this study, 2X, 3X, and 4X wheels are compared. These wheels have

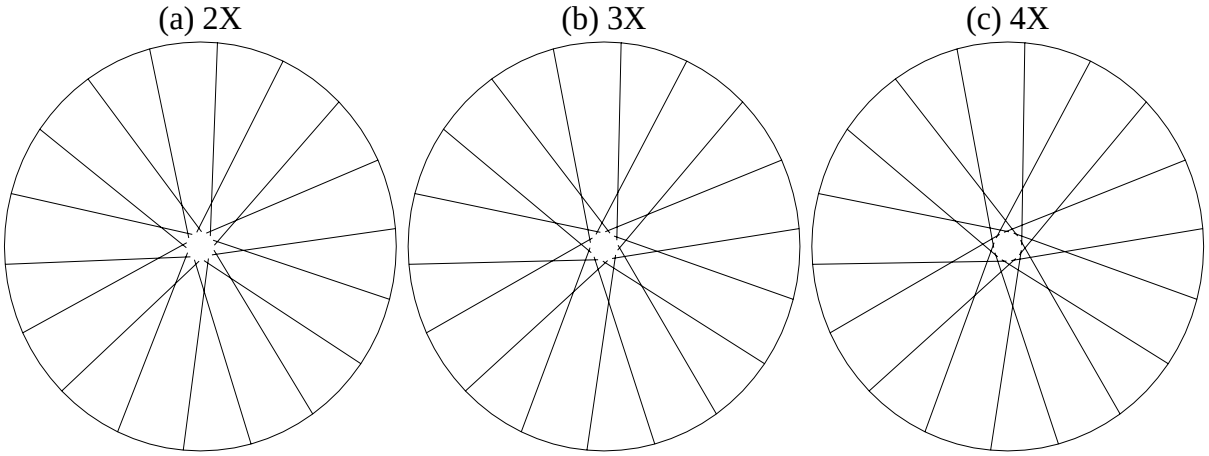

FIG. 1. Spoke lacing geometries: (a) 2X**; (b)** 3X**; (c)** 4X

equal numbers of "pulling" spokes (which increase in tension under torsional pedaling loads applied at the hub) and "pushing" spokes (which lose tension under torsional pedaling loads).

Bicycle rims are not prismatic, but are periodically perforated by reinforced holes used for the spoke connections. To assess the effective moments of inertia of the rim used in this study, analytical force-deflection relationships of the bare rim were fit in a least-squares sense to experimental force-deflection data. To evaluate the effective bending moment of inertia about the axis parallel to the axle, I_{zz}, the bare rim was loaded in diametric compression. The radial deflection, Δ_r of a slender circular beam of radius R_r due to a diametric point load, P_r was derived as

$$\Delta_r = \frac{2P_r R_r^3}{E_r I_{zz}} \left(\frac{\pi}{8} - \frac{1}{\pi} \right), \tag{1}$$

where E_r is the elastic modulus of the rim. The stiffness of the rim due to out-of-plane loads determined the torsional moment of inertia, J, and the moment of inertia for bending about the radial axis, I_{rr}. The rim was loaded with different boundary conditions to give an over-determined set of equations for I_{rr} and J. Specifically, the rim was rigidly fixed at two points and loaded in the z direction at mid-span as shown in Figure 2. For the case of a semi-circular arch, ($\theta = \pi/2$ in Figure 2), the principle of virtual work was used to derive the deflection at mid-span, Δ_z, due to a out-of-plane load at mid-span, P_z,

$$\Delta_z = \frac{P_z R_r^3}{8} \left[\frac{1}{E_r I_{rr}} \left(\pi - \frac{4}{\pi} \right) + \frac{1}{GJ} \left(3\pi - 8 - \frac{4}{\pi} \right) \right], \tag{2}$$

which is a linear combination of $1/(E_r I_{rr})$ and $1/(GJ)$. For circular arches of other geometries ($\theta \neq$

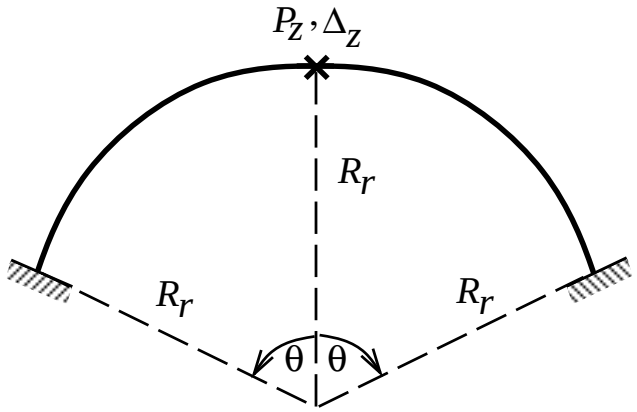

FIG. 2. Geometry of the out-of-plane rim tests.

$\pi/2$), the derivation of the deflection due to a mid-span, out-of-plane, point load was carried out using the principle of virtual work via a symbolic mathematics manipulator, and resulted in cubics in $E_r I_{rr} GJ$ in the numerator and quartics in $E_r I_{rr} GJ$ in the denominator. This non-linear relation was used to determine coefficients $g(\theta)$ and $h(\theta)$ of the linearized approximation:

$$\Delta_z = P_z R_r^3 \left[\frac{g(\theta)}{E_r I_{rr}} + \frac{h(\theta)}{GJ} \right], \tag{3}$$

over a representative range of $E_r I_{rr}$ and GJ. For $70\ \mathrm{Nm}^2 \leq E_r I_{rr} \leq 90\ \mathrm{Nm}^2$ and $10\ \mathrm{Nm}^2 \leq GJ \leq 50\ \mathrm{Nm}^2$, values of $g(\theta)$ and $h(\theta)$ are given in Table 1. The relative error is defined as unity minus the

TABLE 1. Coefficients for equation 3

θ (1)	$g(\theta)$ (2)	$h(\theta)$ (3)	rel. error (4)
$\pi/6$	0.00638	0.000107	0.003
$\pi/4$	0.02322	0.000641	0.004
$\pi/3$	0.05980	0.002391	0.003
$\pi/2$	0.23354	0.018942	10^{-7}
$2\pi/3$	0.6005	0.0987	0.004
$3\pi/4$	0.853	0.202	0.007
$5\pi/6$	1.121	0.387	0.01

ratio of the linearized approximation to the principle of virtual work solution. The coefficients given in Table 1 result in a uniform approximation over the specified range.

Experiments as described by Figure 2 and diametrical compression experiments were carried out to determine the flexibilities $\Delta/(PR^3)$. Figure 3 shows the test data and linear fits for the diametrical case, and cases $\theta = \pi/3$, $\theta = \pi/2$, and $\theta = 2\pi/3$. The rim was rotated between each of the six tests for each of the four configurations. Stiffnesses were taken as the slopes of the straight-line fits, and are given in Figure 3. This data, Table 1, and Equation (3), lead to least-squares approximations for $1/(E_r I_{zz})$, $1/(E_r I_{rr})$, and $1/(GJ)$, which give $E_r I_{zz} = 54.5\ \mathrm{Nm}^2$, $E_r I_{rr} = 82.7\ \mathrm{Nm}^2$, and $GJ = 29.5\ \mathrm{Nm}^2$ with a coefficient of determination greater than 99%.

The three wheels tested have all properties in common, except the spoke pattern (see Table 2). The spokes are made of 304 stainless steel wire and the rims are made of extruded aluminum.

COMPARISON OF ANALYTIC MODELS FOR RIM-SPOKE-HUB SYSTEMS

Assuming negligible lateral rim deflections under a radial load, the radial deflection of the rim, Δ_r, is related to spoke strain, ϵ, by $\Delta_r = \epsilon L_{eff} / \cos\alpha$. The effective (deformable) length of the spoke,

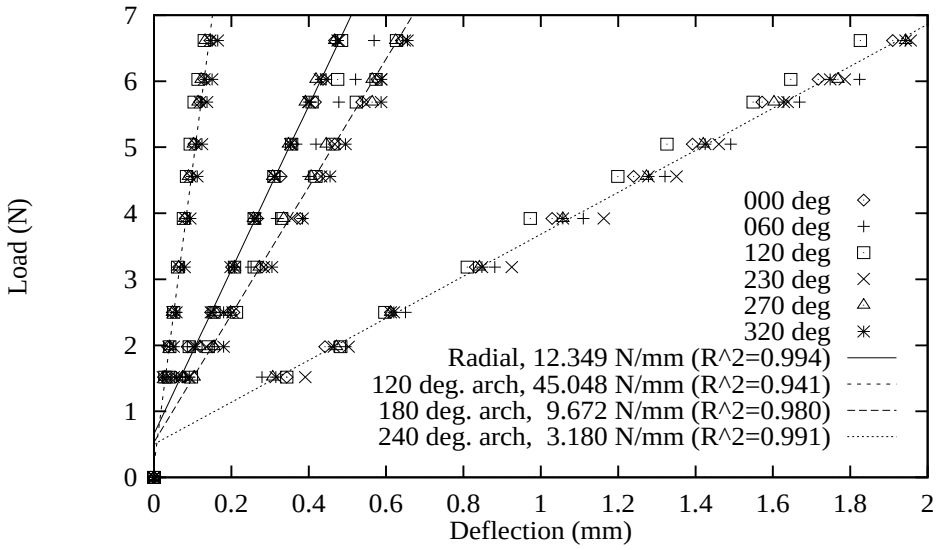

FIG. 3. Force-deflection data for the rim tests.

TABLE 2. Common Properties of Wheels

Property (1)	Symbol (2)	Value (3)
Rim Radius	R_r	309.5 mm
Bending Moment of Inertia	I_{zz}	795 mm^4
Bending Moment of Inertia	I_{rr}	1200 mm^4
Torsional Moment of Inertia	J	1139 mm^4
Hub Flange Radius	R_h	22.2 mm
Plane of Rim to Left Flange	H_L	36.7 mm
Plane of Rim to Right Flange	H_R	14.1 mm
Spoke Diameter	D_s	1.83 mm
Spoke Modulus	E_s	206 GPa
Rim Modulus	E_r	69 GPa
Rim Shear Modulus	G	26 GPa
Number of Spokes	N_s	36 spokes

L_{eff}, is 14.4 mm less than the length of the spoke to the neutral axis of the rim, L, due to the rigid threaded connection between the spoke and the rim. The angle α is the inclination of the spoke to the radius of the wheel. For spokes on the right side of the wheel,

$$\cos\alpha_R = \frac{L_R^2 - H_R^2 + R_r^2 - R_h^2}{2R_r L_R}. \tag{4}$$

Likewise, for spokes on the left side of the wheel, $\cos\alpha_L$ can be evaluated by replacing L_R and H_R with L_L and H_L in Equation 4. The subscripts R and L indicate the right and left sides of the wheel. The angle α reflects an inclination of the spoke both within and out of the plane through the rim. The geometry of a single spoke in relation to the hub and the rim is illustrated in Figure 4.

The theory of circular beams on an elastic foundations has been shown to accurately model the in-plane behavior of spoked bicycle wheels (Burgoyne and Dilmaghanian 1993). In the present study, the

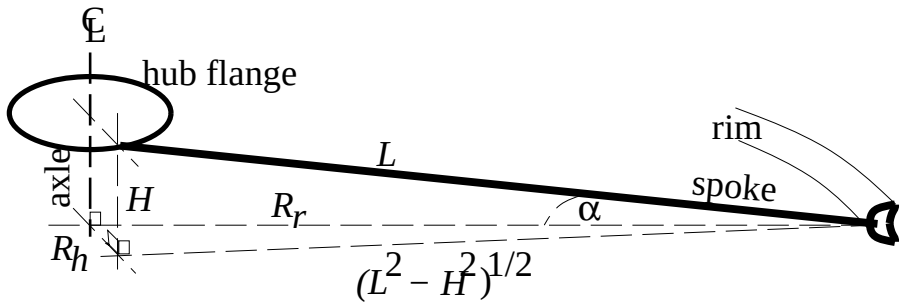

FIG. 4. Geometry of a spoke in relation to the rim and the hub, in three-dimensions.

foundation stiffness per unit length of rim circumference, k, is approximated by

$$k = \frac{N_s E_s D_s^2}{16 R_r} \left(\frac{\cos^2 \alpha_R}{L_{R_{eff}}} + \frac{\cos^2 \alpha_L}{L_{L_{eff}}} \right). \tag{5}$$

The analytic solution adopted in this study for the in-plane deformation of a flexural beam on an elastic foundation, fixed at the center and loaded with a radial point load, is described by M.I. Hetenyi (1956). In Hetenyi's solution, the maximum radial deflection of the rim is:

$$\Delta_r = \frac{P_r R_r^3}{4\alpha\beta E_r I_{zz}} \left(\frac{2\alpha\beta}{\pi\eta^2} - \frac{\beta \sinh \alpha\pi \cosh \alpha\pi + \alpha \sin \beta\pi \cos \beta\pi}{\eta(\sinh^2 \alpha\pi + \sin^2 \beta\pi)} \right), \tag{6}$$

where

$$\eta = \sqrt{\frac{R_r^4 k}{E_r I_{zz}} + 1}, \tag{7}$$

$$\alpha = \sqrt{\frac{\eta - 1}{2}}, \tag{8}$$

and

$$\beta = \sqrt{\frac{\eta + 1}{2}}. \tag{9}$$

The key parameter in Hetenyi's analysis is the ratio of the foundation stiffness to the beam stiffness, $R_r^4 k/(E_r I_{zz})$. Hetenyi's solution is somewhat more simple to evaluate than an analysis presented by Pippard (1931, 1932) that was adopted in a previous study (Burgoyne and Dilmaghanian 1993). Pippard's analysis is useful in analyzing sparsely spoked wheels, or when computational structural analysis methods are not available. Both analyses approximate the spoke system as an elastic foundation of uniform stiffness per unit length.

To evaluate the approximation given by Equations (4), (5) and Hetenyi's equations, radial wheel stiffnesses from the elastic foundation approximation were compared to those calculated by a three-dimensional frame analysis of the rim-spoke-hub system. The first-order elastic frame analysis included out-of-plane bending, axial, and torsional deformation of the rim, and bending deformation of the spokes, since pre-tensioning of the spokes leads to high-friction connections at the rim and hub. In fact, after a period of use, spokes become embedded in the hub flange. Calculated spoke moments were always less than 1% of the rim moments. Torsional, axial, and out-of-plane bending of the rim are not included in the elastic foundation analysis. Different spoke sizes, inertias I_{zz}, and lacing patters were analyzed. All other wheel parameters were held at the values given in Table 2.

The frame analysis gave 5% to 7% lower radial stiffnesses than did the elastic foundation analysis, as shown in Figure 5. The effect of the spoke pattern is similar in the two analysis methods. For both methods, the 2X wheel is 1.7% more stiff than the 3X wheel, and the 4X wheel is 1.8% less stiff than the 3X wheel. The spoke pattern affects the over-all stiffness more than it affects the spoke strains. For both methods, the spoke strains of the 2X wheel and the 4X wheel are within 1% of the 3X wheel.

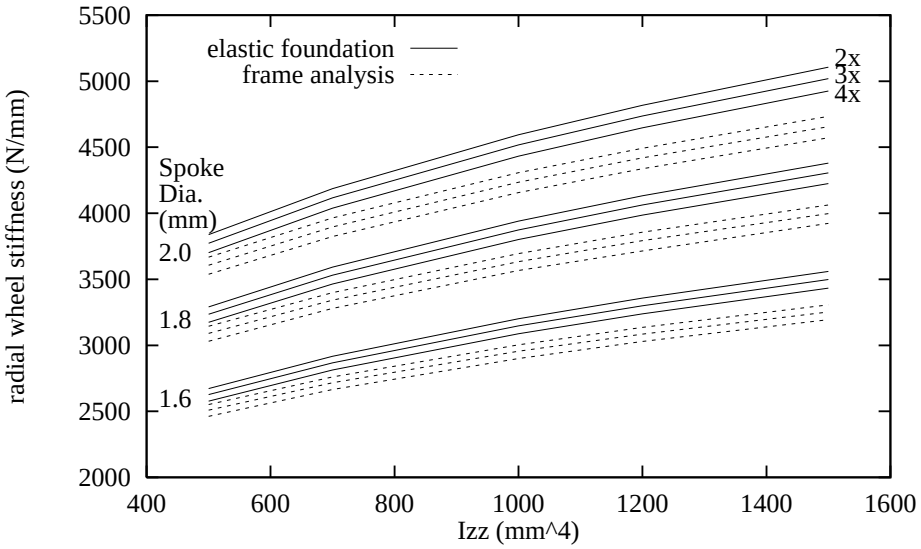

FIG. 5. Radial stiffness for various bicycle wheel designs. Continuous elastic foundation solution: —–; Elastic frame analysis: - - - -.

Deflections due to lateral point loads and tangential point loads on the rim were computed using the three-dimensional frame model. The resulting stiffnesses are given in Figures 6 and 7. Wheels with

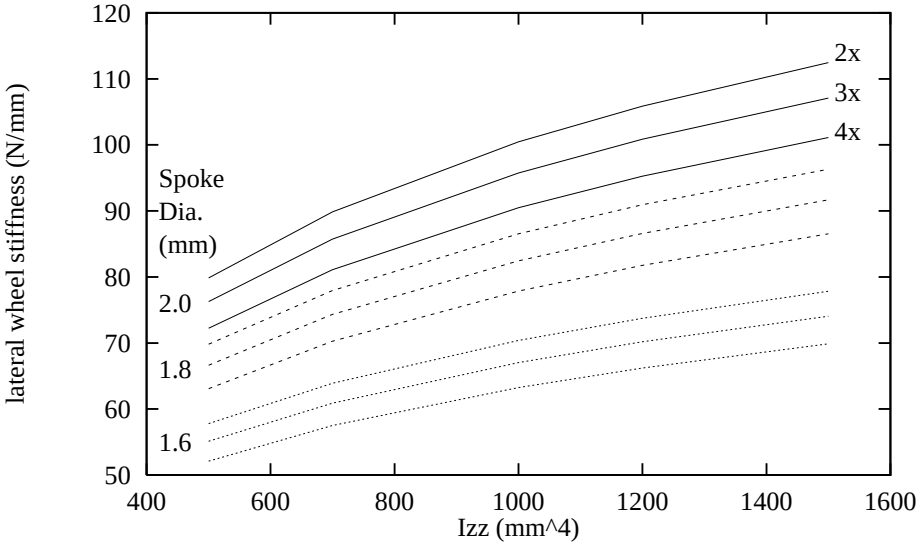

FIG. 6. Lateral stiffness for various bicycle wheel designs.

longer spokes (4x) are more flexible to radial and lateral loads. The 4x wheel is most stiff to tangential (braking and accelerating) loads on the rim. Careful experiments on wheels that were identical except for the spoke pattern, gave similar variations in radial, lateral, and tangential stiffness due to changes in the spoke pattern (Price and Akers 1985).

The strains in spokes adjacent to the loading point do not follow the same trends as do the wheel stiffnesses. The strains in a right pulling spoke were calculated using the three-dimensional elastic model with radial, lateral, and tangential loads applied at the rim-spoke node. The strain sensitivities

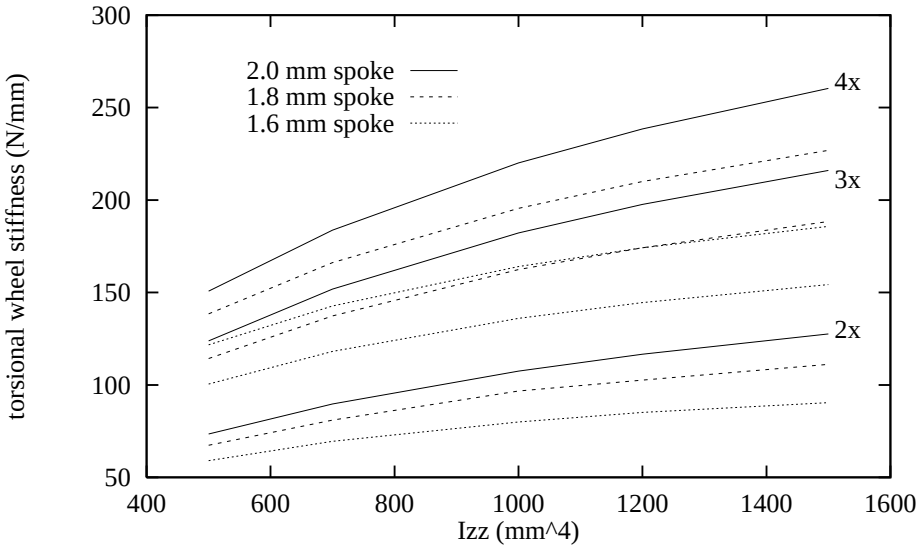

FIG. 7. Tangential stiffness for various bicycle wheel designs.

are given in Table 3. Wheel properties are those given in Table 2. Wheels with shorter spokes (2x) have

TABLE 3. Spoke strains in a right pulling spoke due to radial, lateral, and tangential loads to the rim, via an elastic frame analysis

Load Type (1)	2x ($\mu\epsilon$/N) (2)	3x ($\mu\epsilon$/N) (3)	4x ($\mu\epsilon$/N) (4)
radial	0.975	0.989	0.988
lateral	1.128	0.887	0.811
tangential	3.124	3.151	3.183

significantly higher spoke strains when lateral loads are applied to the rim. Under radial and tangential loads, wheels with shorter spokes have somewhat lower spoke strains.

STATIC SPOKE STRAIN MEASUREMENTS

Strains in a right pulling spoke from each wheel were measured by a pair of 120Ω strain gauges occupying a single 240Ω arm of a Wheatstone bridge, which included a similarly gauged temperature compensation arm. The gages used were Micro-Measurements EA-13-23005-120 gages, with gage grid dimensions of 5.84 mm by 0.56 mm. The temperature compensation gauges were placed on a 10 cm length of spoke which remained unstressed during testing. This gauge configuration was insensitive to bending strains and decreased the resistive heating of the gauges (Gavin 1986). The measurement circuit exhibited micro-volt stability and measurements were accurate to within $\pm 2\mu\epsilon$. The circuit sensitivity was determined by the shunt calibration method. The sensitivity was confirmed by a test for the elastic modulus of the compensation arm of the bridge, which resulted in a modulus of 210 GPa (Gavin 1986).

Tests to evaluate the effect of a radial load on the spoke strains were limited to static service load levels. A single radial load applied to the axle ranged from 200 N to 450 N. The gauged spoke was located between the hub and the ground and tests were carried out using wheels with tires inflated to 700 kPa. Figure 8 illustrates the results of the static tests and a linear curve-fit for each wheel type. Each curve-fit was constrained to pass through the origin. The slope of each curve-fit is tabulated in the legend of Figure 8. Spoke lengths are as follows: 2x: 295.4 mm & 293.2 mm; 3x: 301.4 mm & 299.4 mm; 4x: 308.4 mm & 306.8 mm. Only minor variations in the spoke-strain sensitivity are

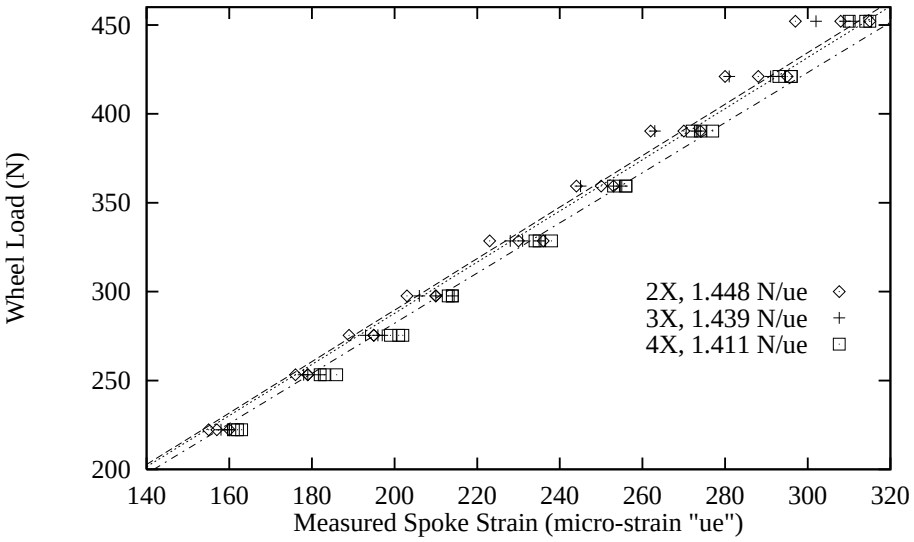

FIG. 8. Effect of static load and lacing pattern on spoke strain with an ordinary least squares fit to the data.

observed among the three wheel types. Strains in the 2X wheel are somewhat less than strains in the 4X wheel. The tire transfers forces from the rim to the ground through deformation of, and loss of pre-tension in, the tire walls (Burgoyne and Dilmaghanian 1993). The load-distributing effect of the inflated tire resulted in measured spoke strains that were lower than those given in Table 3. A slight non-linearity is illustrated in Figure 8. Similar non-linear behavior in another study was attributed to slackening of the spokes (Burgoyne and Dilmaghanian 1993). At higher radial loads, spokes lose tension at a decreasing rate per unit radial load. As spokes lose tension, loads are carried to a greater extent by moments in the rim. While these experiments show a slight increase in spoke-strain with spoke length, the analytical methods show a slight reverse trend. Therefore, from laboratory, three-dimensional analyses, and analytical solutions, it may only be concluded that static spoke strain due to radial loads are roughly independent of the spoke pattern, for the wheels in this study. Static spoke strains are, however, influenced by the spoke pattern when lateral loads are applied to the rim. In this case, wheels with the shortest spokes have the highest spoke strains.

ROAD TESTS

Under service conditions, spoke strains respond to lateral (cornering), tangential (accelerating and braking), as well as radial (gravity) loads on the rim. The variability of loading conditions introduces variability in the spoke strain. To collect road test spoke strain records, the strain signal was balanced and amplified by a custom, wheel-borne circuit prior to transmission through carbon/silver slip-rings, in order to mitigate the effects of slip-ring noise. Figure 9 shows the test assembly. The road test circuit was comprised of a 2-arm, 4-gauge Wheatstone bridge, two 240 Ω precision resistors for bridge completion, an integrated circuit instrumentation amplifier to improve the signal to noise ratio, two micro-potentiometers to balance the Wheatstone bridge and zero the amplifier bias error, a precision shunt calibration resistor, two 9 volt batteries for the amplifier, a 1.3 volt battery for the strain gauges, and micro dip-switches to turn on power to the bridge, amplifier, to select amplifier gains, and to insert the shunt calibration resistor in parallel with the measurement arm of the bridge. Bending of the pedal crank-arm was also measured during the road tests with a similar circuit. Shunt calibration was performed before and after collecting data from each wheel. The strain data was transmitted to an instrumentation vehicle via cable, and was recorded in FM on magnetic tape in three 10 minute segments, one for each wheel. The data was subsequently digitized at 500 samples per second for analysis. The same 4 km loop, which included a variety of road conditions, was covered three times for each wheel. In an

FIG. 9. Wheel-borne road test circuit, showing instrumentation amplifier, slip-rings, and battery supply.

effort to record the largest reasonable variation in spoke strains, obstacles, such as potholes, were not avoided. Figure 10 illustrates the nature of the spoke strain under actual riding conditions. Negative strain indicates a prestress loss. The total weight of the bicycle and rider was 930 N.

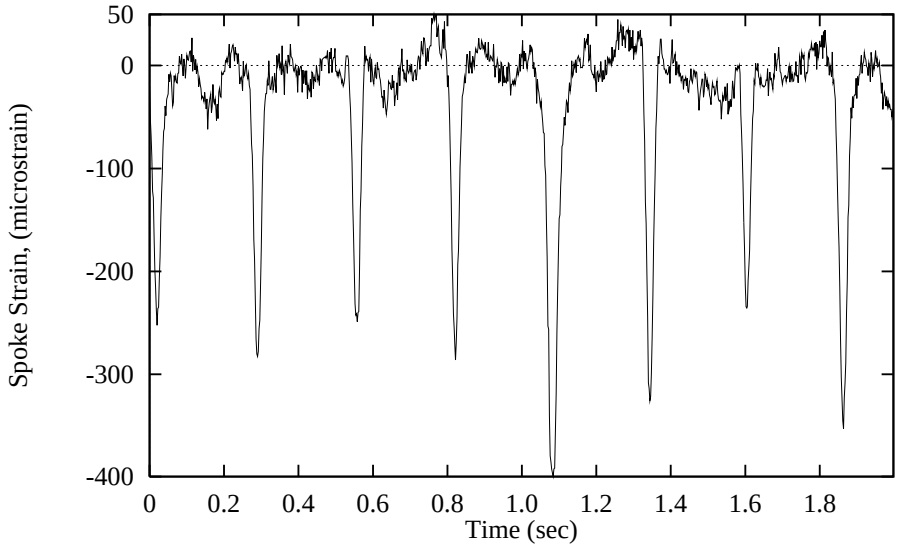

FIG. 10. Measured spoke strain time history during actual riding conditions.

DATA REDUCTION

Due to the random nature of the strain records, segments of the records corresponding to a single wheel revolution were averaged for each wheel. Only portions of the digitized records that contained smooth and periodic spoke strains were averaged. Bias errors were subtracted before averaging. The average strain over a single revolution is plotted in Figure 11. The small oscillations with a 40° period are attributed to the four-spoke grouping, which is characteristic of 36-spoke wheels. Also shown in

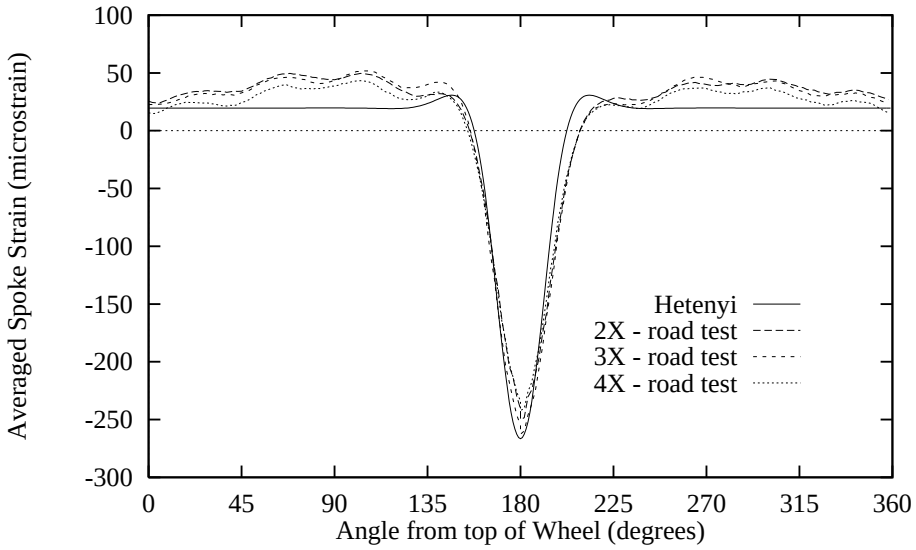

FIG. 11. Average strain of a right pulling spoke as it circles the wheel under actual riding conditions.

Figure 11 is the result of Hetenyi's analysis for a distributed load applied to the rim (to account for the effect of the tire).

To simulate the transfer of load between the ground and the rim (through the deformed tire) in Hetenyi's analytic model, five (fictitious) point loads were applied symmetrically over a twenty degree arc of the rim. Since the load distributing effect of the tire, through deformation of the tire side-walls, could not be measured easily during road tests, the three interior loads, P_i, were assumed to be equal, with two smaller out-lying point loads, P_o, equal to each other. For a given total load, $3P_i + 2P_o$, the maximum rim deflection depends on the ratio (P_o/P_i). This ratio was selected to reproduce the measured spoke strains of the 3X wheel from the static laboratory experiments (1.439 N/$\mu\epsilon$), which resulted in $(P_o/P_i) \approx 0.77$.

The weak dependence of strain on the spoke pattern is predicted by both linear analytical solutions and the low-level static tests. Changes in spoke length and spoke pattern (in the range of values in this study) do not influence Hetenyi's results or a elastic frame analysis significantly. Pippard's studies on spoked wheels with high foundation to rim stiffness ratio ($R_r^4 k/(E_r I_{zz}) \approx 2000$), and nearly radial spokes ($\alpha < 10°$) show that spoke tensions are significantly sensitive ($> 5\%$) to α only under loads tangential to the rim (accelerating and braking) (Pippard and Francis 1932; Pippard and White 1932). Spoke strains decrease with increasing α under tangential loads (Table 3, Pippard and White 1932) and lateral and torsional loads are typically low under steady pedaling in a straight line. Laboratory tests and analysis show that changes in the spoke strain sensitivity to radial loads are $15\mu\epsilon/\mathrm{kN}$ from one wheel to another. Similar variations shown in Figure 11 are probably due to variations in the loading conditions. Lateral and tangential static loads on the rim are typically small during steady cycling.

SPOKE STRAIN STATISTICS AND FATIGUE LIFE ASSESSMENT

To evaluate the cumulative probability distribution (CDF) of spoke strain cycles, $F_\epsilon(\epsilon_i)$, the magnitude of the maximum strain cycle, ϵ, was extracted for each wheel revolution, i, ($i = 1 \ldots N_{test}$), and sorted in order of increasing ϵ ($\epsilon_1 < \ldots < \epsilon_i < \ldots < \epsilon_{N_{test}}$). The CDF of the spoke strain is $F_\epsilon(\epsilon_i) = i/(N_{test} + 1)$, and is illustrated in Figure 12. The averages and sample standard deviations (std. dev.) of these distributions are given in Table 4. The extreme measured spoke strains were about 600 $\mu\epsilon$, which corresponds to a spoke stress range of 150 MPa. These stress cycles were probably due to traversing a pothole, which were not avoided in the road tests.

The number of cycles to fatigue failure, N, for a constant stress range, S, is assumed to be a log-

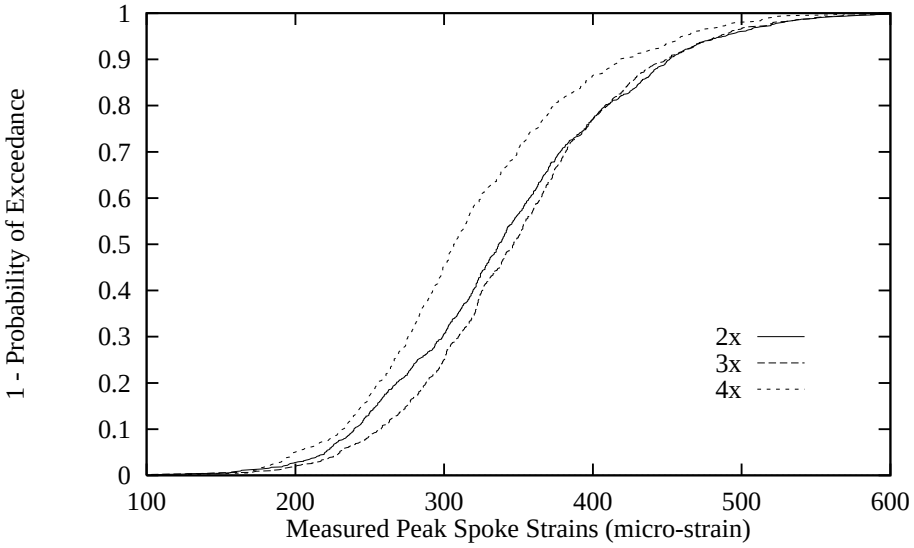

FIG. 12. Cumulative distribution function of spoke strain cycle amplitudes.

TABLE 4. Statistics of the Spoke Strain CDF.

Wheel Type (1)	N_{test} (cycles) (2)	average ϵ ($\mu\epsilon$) (3)	std. dev. ϵ ($\mu\epsilon$) (4)
2x	1087	342	82
3x	901	349	76
4x	551	317	74

normally distributed random variable (Fuchs and Stephens 1980, Pope 1959), which satisfies the relation

$$\log S = a \log N + b. \tag{10}$$

In other words, $N = 10^{b/a} S^{1/a}$. Equation 10 presumes that there is no threshold stress range below which no fatigue accumulates. This assumption is conservative since very low stress cycles usually do not contribute to the accumulation of fatigue damage. In 1984 and 1985, fatigue tests on stainless steel bicycle spokes were carried out for Wheelsmith, Inc. at Stanford University. Constant cycle tests were conducted with pre-tensioning stresses of 174 MPa, 250 MPa, 343 MPa, 347 MPa, 424 MPa, and 501 MPa. Any correlation between the cycles to failure, N, and the pre-tensioning stress was obscured by random variations in N. The parameters a and b were determined from a least squares fit of fatigue data from 76 stainless steel bicycle spokes, shown in Figure 13 (using N as the dependent variable (Rice 1985)). Variations in the (dependent) variable N due to stress cycles of a constant amplitude, S, are modeled by the normally distributed random variable b, with average $\bar{b}$, and coefficient of variation V_b. For the data shown in Figure 13, a=-0.30 log(MPa)/log(cycle), $\bar{b}$=4.12 log(MPa), V_b=0.017. Using this data, the coefficient of variation of N is 0.74, for any constant value of S. This data is unique to the spoke material, the spoke geometry, and the spoke's particular stress concentrations. In 68 spokes the failure occurred at the cold-worked elbow; in the remaining 8 spokes the failure occurred at the threads.

The smallest stress cycle in the fatigue tests was 174 MPa, whereas the stress range from the road test data was 20 MPa to 150 MPa. Hence, the fatigue data was extrapolated to the low stress range. (To have tested a single sample at 40 MPa would have required over a year of continuous testing at 10 cycles per second, and an unwarranted use of facilities.) Assuming a linear fatigue damage accumulation model, each stress cycle of stress range S contributes $1/N(S)$ to fatigue failure. For example, each cycle at

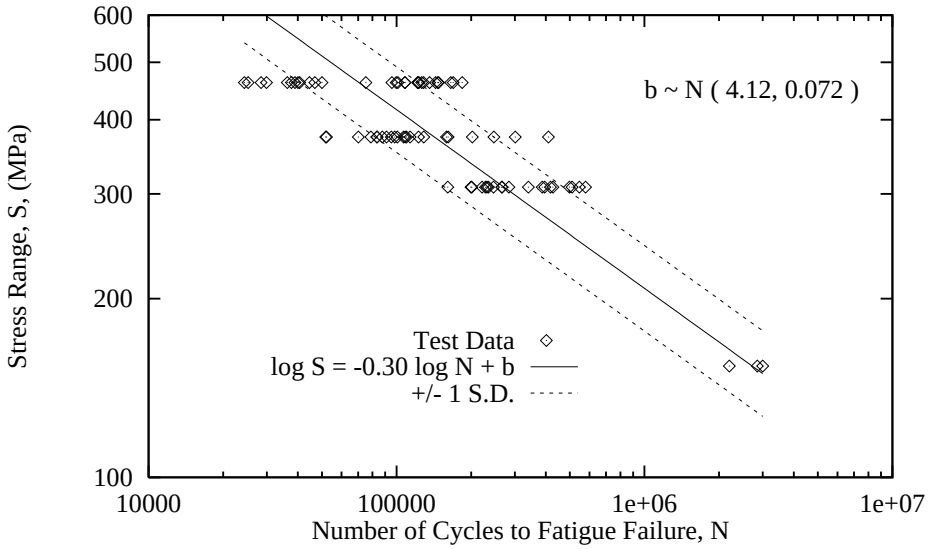

FIG. 13. Bicycle spoke fatigue failure data.

the largest spoke stress cycle (150 MPa) shortens the remaining fatigue life by about one one-millionth of the total fatigue life, on average. The linear fatigue damage accumulation model neglects interaction between cycles of different stress levels in complex loading histories (Yen 1969). Because the fatigue loading cycles are regular and of a roughly uniform amplitude, a linear fatigue damage accumulation model is applicable to spoke fatigue (Fuchs and Stephens 1980). In N_{life} wheel revolutions, the number of cycles of stress in the interval $[S_i, S_{i+1}]$ is given by $n_i = N_{life}/(N_{test}+1)$, where $S_i = E_s\epsilon_i$ and ϵ_i is the i^{th} element of the set of ordered spoke strains. A *damage index*, $\mathcal{D}$, is defined by

$$\mathcal{D} = \sum_{i=1}^{N_{test}} \frac{n_i}{N(S_i)}, \tag{11}$$

which can be expressed as

$$\mathcal{D} = 10^{b/a} E_s^{-1/a} \frac{N_{life}}{N_{test}+1} \sum_{i=1}^{N_{test}} \epsilon_i^{-1/a}, \tag{12}$$

and is a log-normally distributed random variable. The probability of fatigue failure, P_f, is the probability that $\mathcal{D}$ exceeds $\mathcal{D}_f$, $P_f = \Phi((\log \mathcal{D}_f - E[\log \mathcal{D}])/\sigma_{\log \mathcal{D}})$, where Φ represents the standard normal CDF , E is the expectation operator, and $\sigma_{\log \mathcal{D}}$ is the standard deviation of $\mathcal{D}$, which follows directly from Equation 12. For fatigue stress cycles of constant amplitude $\mathcal{D}_f = 1.0$. In fatigue tests with ascending stress amplitudes, failure is often observed when $\mathcal{D}_f > 1$, and with descending stress amplitudes $\mathcal{D}_f < 1$ (Pope 1959). A conservative value of $\mathcal{D}_f$ of 0.3 has been recommended for random in-service fatigue loadings (Leve 1969).

Cycles with the largest spoke strain have the largest contribution to P_f. The CDF of spoke strain for the wheels entire life, ($F_\epsilon(\epsilon_i)$ for N_{life} cycles) is assumed to be equal to the measured $F_\epsilon(\epsilon_i)$ for N_{test} cycles. This assumption leads to an underestimate for P_f, but extrapolation of irregular measured CDF's is tenuous. Figure 14 illustrates the sensitivity of the likelihood of spoke fatigue failure with respect to service life. Relationships for $\mathcal{D}_f = 0.3$ and $\mathcal{D}_f = 1.0$ are shown. In evaluating Equation 12 for Figure 14, the measured spoke strains for all three wheels were combined. For a standard bicycle wheel, 472 cycles corresponds to 1 km. Riding across the continental United States corresponds to 3.8 million cycles. Riding 50 km every day for one year corresponds to 8.6 million cycles. This study shows that bicycle wheels intended for mileage comperable to a cross-country excursion are very reliable with respect to radial fatigue loads.

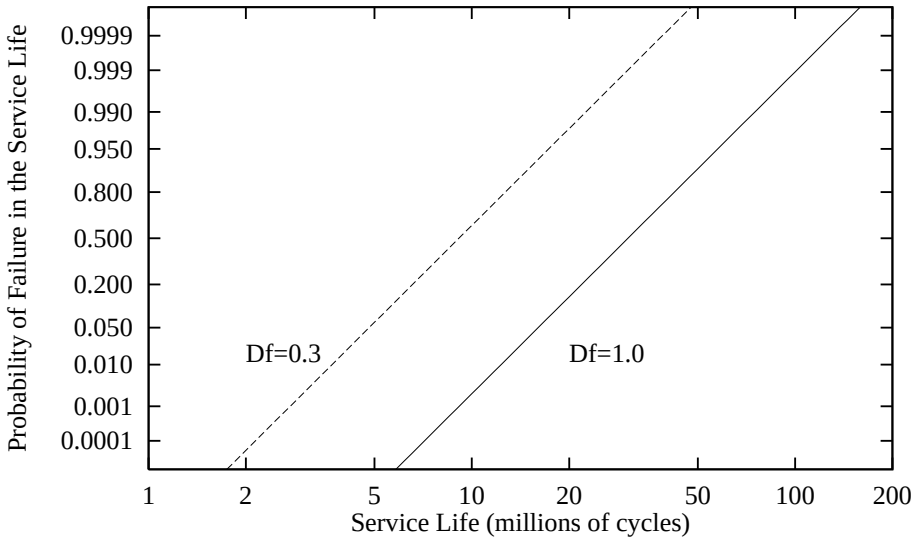

FIG. 14. Increase in the probability of spoke failure with service life.

Since the failure of one spoke renders the wheel un-serviceable, the spoke system is considered to be a series system of N_s elements with identically distributed fatigue resistances. If the spoke fatigue resistances are perfectly correlated, then the probability of fatigue failure for the wheel is P_f for a spoke. If the spoke fatigue resistances are uncorrelated, then probability of fatigue failure for the wheel is $1-(1-P_f)^{N_s}$. If P_f for a spoke is 0.001 then the failure probability for a 36 spoke wheel is between 0.001 and 0.035.

CONCLUSIONS

Requirements of strength, stiffness, and low weight are satisfied in bicycle wheels by combining a light-weight rigid rim with pre-tensioned wire spokes. In many rear wheels very high pre-tension stresses in half the spokes are required to maintain an asymmetrical shape. The radial, lateral, and tangential stiffness of wheels with various spoke sizes, spoke geometries and rim stiffnesses is presented. The behavior of bicycle wheels subjected to static radial loads can be accurately modeled by idealizing the system of interlacing spokes as a linear elastic foundation of uniform stiffness per length of circumference. The spoke pattern affects the over-all radial stiffness of the wheel more than it affects the spoke strains. From a theoretical analysis, a numerical analysis, static experimental analysis, and in-service measurements, the spoke strains appear to be insensitive to the pattern of the spoke lacing. From a numerical analysis, the spoking pattern has the greatest impact on the spoke strains when the wheel is subjected to large lateral loads, such as during cornering. In this case, wheels with longer spokes have lower strains than do wheels with shorter spokes. Small variations in measured spoke strains between the wheel types under actual riding conditions, are attributed to variations in un-measured loads. The extreme spoke stress cycles in the road test experiments were on the order of 150 MPa. Each cycle at this stress level shortens the remaining fatigue life by one one-millionth of the total fatigue life. Larger stress cycles, due to large lateral loads, for instance, could shorten the fatigue life considerably. Future work could therefore be directed toward:

- Measurements of spoke strains due to high lateral loads, and,
- Non-linear modeling of spoked wheels subjected to spoke-slackening loads.

The fatigue resistance of the spokes, the spoke diameter, the arrangement of the spokes, and the stiffness of the rim influence wheel stiffness and fatigue life. Wheels with 2X, 3X, and 4X spoke patterns all have similar spoke strains when subjected to radial loads. The fatigue resistance of spoked wheels to steady cycling loads is very high for most typical service conditions.

ACKNOWLEDGMENTS

The results of a detailed study by C.J. Burgoyne and R. Dilmaghanian (1993) shed insight into the elastic behavior of spoked bicycle wheels. The guidance of Professor Robert Mark of Princeton University, and the technical assistance of Rod Rowland, formerly of Princeton University, were invaluable in carrying out the experiments described in this paper. The author is grateful for conversations with Jim Papadopoulos regarding the road test data. Bob Flower of Bike Tech Magazine and Jon Hjertberg of Wheelsmith, Inc. graciously provided test specimens for the original study and fatigue data.

APPENDIX I. REFERENCES

Burgoyne, C.J. and Dilmaghanian, R. (1993) "Bicycle Wheel as Prestressed Structure." *Journal of Engineering Mechanics,* 119(3), pp. 439-455.

Fuchs, H.O. and Stephens, R.I. (1980) *Metal Fatigue in Structures.* New York: John Wiley and Sons.

Gavin, H.P. (1986) "Spoked Bicycle Wheels: A Comparative Experimental and Finite Element Analysis of Static and Dynamic Characteristics of Bicycle Wheels with Variable Spoking Patterns." *Undergraduate Thesis,* Dept. of Civil Eng., Princeton University, Princeton, N.J.

Hetenyi, M.I. (1956) *Beams on Elastic Foundation.* University of Michigan Press, Ann Arbor, MI. pp. 156–163.

Leve, Howard L. (1969) "Cumulative Damage Theories." in *Metal Fatigue: Theory and Design.* A.F. Madayag ed. New York: John Wiley and Sons.

Pippard, A.J.S., and Francis, W.E. (1931) "The stresses in a radially-spoked wire wheel under loads applied to the rim." *Philosophical Magazine,* 7(11), 233-285.

Pippard, A.J.S., and Francis, W.E. (1932) "The stresses in a wire wheel under side loads on the rim." *Philosophical Mag.,* 7(14), 436-445.

Pippard, A.J.S., and White, M.J. (1932) "The stresses in a wire wheel with non-radial spokes under loads applied to the rim." *Philosophical Mag.,* 7(14), 209-233.

Pope, Joseph Albert. (1959) *Metal Fatigue.* London: Chapman and Hall.

Price, D. and Akers, A. (1985) "Stiffness Characteristics of Bicycle Wheels." *Bike Tech.* Emaus, PA: Rodale Press. Vol. 4, No. 3, June 1985. pp 1-7.

Rice, Richard C. (1985) "Fatigue Data Analysis." in *Metals Handbook.* 9th Edition, Vol. 8 (Mechanical Testing), Metals Park, Ohio: American Society for Metals.

Yen, Charles S. (1969) "Interpretation of Fatigue Data." in *Metal Fatigue: Theory and Design.* A.F. Madayag ed. New York: John Wiley and Sons.

APPENDIX II. NOTATION

The following symbols are used in this paper:

a, b = empirical coefficients for fatigue life prediction;
$\bar{b}$ = average value of b;
$\mathcal{D}$ = damage index;
$\mathcal{D}_f$ = value of $\mathcal{D}$ at failure;
D_s = spoke diameter (1.6 mm, 1.8 mm, 2.0 mm);
E_r = rim modulus of elasticity;
E_s = spoke modulus of elasticity;
$F_\epsilon(\epsilon_i)$ = probability that $\epsilon \leq \epsilon_i$;
G = shear modulus of the rim;
g, h = coefficients in a linearized model for lateral arch deflections;
H_L = distance from a plane through the rim to the left side of the hub;
H_R = distance from a plane through the rim to the right (gear) side of the hub;
I_{rr} = bending moment of inertia of the rim about its neutral axis parallel to the radius;
I_{zz} = bending moment of inertia of the rim about its neutral axis parallel to the axle;
J = torsional moment of inertia of the rim;
k = foundation stiffness of the system of interlacing spokes;
L_L = length of a spoke on the left side of the hub to the neutral axis of the rim;
L_R = length of a spoke on the right (gear) side of the hub to the neutral axis of the rim;
$L_{L_{eff}}$ = effective length of a spoke on the left side of the hub ($L_L - 14.4\text{mm}$);
$L_{R_{eff}}$ = effective length of a spoke on the right side of the hub ($L_R - 14.4\text{mm}$);
N = number of stress cycles to fatigue failure;
N_{life} = service life of a wheel (cycles);
N_{test} = number of wheel revolutions in a measured record of spoke strains;
n_i = number of measured cycles of stress in the range $[S_i, S_{i+1}]$;
N_s = number of spokes in the wheel;
P_f = probability of fatigue failure, probability that $\mathcal{D} \geq 1$;
P_r, P_z = radial and lateral point loads applied to the rim;
R_r = radius to the neutral axis of the rim;
R_h = radius to the spoke holes in the flange of the hub;
S = stress range of a fatigue stress cycle;
V_b = coefficient of variation of b;
$\sigma_{\log \mathcal{D}}$ = standard deviation of $\log \mathcal{D}$;
α_R = angle of a spoke on the right side of the wheel to the wheel's radius;
α_L = angle of a spoke on the left side of the wheel to the wheel's radius;
Δ_r = radial rim deflection due to a radial point load;
Δ_z = lateral rim deflection due to a lateral point load;
ϵ = strain in a spoke;
θ = half the angle subtended by a circular arch;
Φ = the standard normal cumulative distribution function;
Ω = ohm, unit of electrical resistance.